Inorg. Chem. **2005**, *44*, 5562–5570

Normal-Mode Analysis of $FeCl_4^-$ and $Fe_2S_2Cl_4^{2-}$ via Vibrational Mössbauer, Resonance Raman, and FT-IR Spectroscopies

Matt C. Smith,[†] Yuming Xiao,[†] Hongxin Wang,[†,‡] Simon J. George,[‡] Dimitri Coucouvanis,[*,§] Markos Koutmos,[§] Wolfgang Sturhahn,[||] Ercan E. Alp,[||] Jiyong Zhao,[||] and Stephen P. Cramer[*,†,‡]

Department of Applied Science, University of California, Davis, California 95616, Physical Biosciences Division, Lawrence Berkeley National Laboratory, Berkeley, California 94720, Department of Chemistry, University of Michigan, Ann Arbor, Michigan 48109, and Advanced Photon Source, Argonne National Laboratory, Argonne, Illinois 60439

Received December 10, 2004

$[NEt_4][FeCl_4]$, $[P(C_6H_5)_4][FeCl_4]$, and $[NEt_4]_2[Fe_2S_2Cl_4]$ have been examined using ^{57}Fe nuclear resonance vibrational spectroscopy (NRVS). These complexes serve as simple models for Fe–S clusters in metalloproteins. The ^{57}Fe partial vibrational density of states (PVDOS) spectra were interpreted by computation of the normal modes assuming Urey–Bradley force fields, using additional information from infrared and Raman spectra. Previously published force constants were used as initial values; the new constraints from NRVS frequencies and amplitudes were then used to refine the force field parameters in a nonlinear least-squares analysis. The normal-mode calculations were able to quantitatively reproduce both the frequencies and the amplitudes of the intramolecular-mode ^{57}Fe PVDOS. The optimized force constants for bending, stretching, and nonbonded interactions agree well with previously reported values. In addition, the NRVS technique also allowed clear observation of anion–cation lattice modes below 100 cm^{-1} that are nontrivial to observe by conventional spectroscopies. These features were successfully reproduced, either by assuming whole-body motions of point-mass anions and cations or by simulations using all of the atoms in the unit cell. The advantages of a combined NRVS, Raman, and IR approach to characterization of Fe–S complexes are discussed.

Introduction

Fe−S clusters are ubiquitous in bioinorganic chemistry.[1,2] They serve not only as electron-transfer agents and structural components for metalloenzymes, but also as catalysts in their own right.[3−5] These clusters and relevant model compounds have been intensely studied by a wide variety of spectroscopies, including Mössbauer, NMR, EPR, ENDOR, and EXAFS, and more recently by S K-edge, Fe L-edge, and XMCD analyses. Numerous theoretical studies, involving both molecular mechanics[6] and DFT calculations,[7,8] have sought to explain their electronic and catalytic properties. Nevertheless, the wealth of recent publications[9] demonstrates that, even for the simple 1Fe rubredoxins,[10] 2Fe ferredoxins,[11] and Rieske proteins,[12] there is still much to be learned.

Vibrational techniques, including FT-IR and especially resonance Raman spectroscopies, are powerful probes of the core structure and external ligation of Fe−S clusters in proteins. Mononuclear Fe in rubredoxins, 2Fe clusters in ferredoxins and Rieske proteins, and 3Fe and 4Fe clusters

* To whom correspondence should be addressed. E-mail: spcramer@ucdavis.edu (S.P.C.), dcouc@umich.edu (D.C.).
[†] University of California, Davis.
[‡] Lawrence Berkeley National Laboratory.
[§] University of Michigan.
[||] Argonne National Laboratory.

(1) Rees, D. C.; Howard, J. B. *Science* **2003**, *300*, 929−931.
(2) Rees, D. C. *Annu. Rev. Biochem.* **2002**, *71*, 221−246.
(3) Johnson, M. K. *Curr. Opin. Chem. Biol.* **1998**, *2*, 173−181.
(4) Lindahl, P. A. *Biochem.* **2002**, *41*, 2097−2105.
(5) Drennan, C. L.; Peters, J. W. *Curr. Opin. Struct. Biol.* **2003**, *13*, 220−226.
(6) Ergenekan, C. E.; Thomas, D.; Fischer, J. T.; Tan, M. L.; Eidsness, M. K.; Kang, C.; Ichiye, T. *Biophys. J.* **2003**, *85*, 2818−2829.
(7) Noodleman, L.; Lovell, T.; Liu, T.; Himo, F.; Torres, R. A. *Curr. Opin. Chem. Biol.* **2002**, *6*, 259−273.
(8) Vrajmasu, V. V.; Münck, E.; Bominaar, E. L. *Inorg. Chem.* **2004**, *43*, 4867−4879.
(9) Frazzon, J.; Dean, D. R. *Curr. Opin. Chem. Biol.* **2003**, *7*, 166−173.
(10) Bonomi, F.; Eisdness, M. K.; Iametti, S.; Kurtz, D. M., Jr.; Mazzini, S.; Morleo, A. *J. Biol. Inorg. Chem.* **2004**, *9*, 297−306.
(11) Meyer, J. *FEBS Lett.* **2001**, *509*, 1−5.
(12) Iwasaki, T.; Kounosu, A.; Kollling, D. R. J.; Crofts, A. R.; Dikanov, S. A.; Jin, A.; Imai, T.; Urushiyama, A. *J. Am. Chem. Soc.* **2004**, *126*, 4788−4789.

10.1021/ic0482584 CCC: $30.25
Published on Web 06/11/2005

Chart 1. Anion Structures in (Left) $[NEt_4][FeCl_4]$, (Right) $[P(C_6H_5)_4][FeCl_4]$,[a] and (Bottom) $[NEt_4]_2[Fe_2S_2Cl_4]$

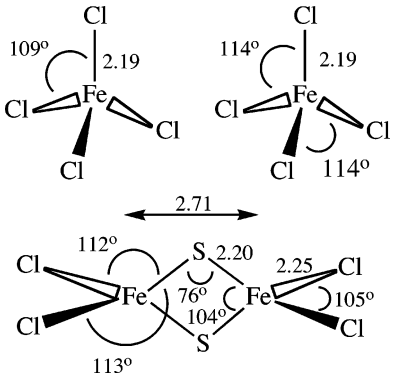

[a] In $[P(C_6H_5)_4][FeCl_4]$, the remaining unlabeled Cl−Fe−Cl angles are 107°. All distances are in angstroms.

in ferredoxins and Hi-PIPs all have characteristic Raman bands. The spectra are also sensitive to the type of side chain as well as its protonation state and conformation with respect to the Fe. Despite the proven strengths of resonance Raman spectroscopy, some samples have resisted characterization—specifically, the $MoFe_7S_8$ and Fe_8S_9 M and P clusters of nitrogenase (N_2ase), as well as the Ni−Fe and H clusters of hydrogenase (H_2ase).

The relatively new technique of nuclear resonance vibrational spectroscopy (NRVS) has great potential for determining the normal modes of inorganic materials.[13,14] It is especially useful for observing the low-frequency motions of Fe−S clusters in proteins, which are obscured by protein bands in IR absorption and not always resonance-enhanced in Raman scattering. NRVS involves different and often less restrictive selection rules than infrared or resonance Raman spectroscopy: the primary requirement is motion of the resonant nucleus (in this case, ^{57}Fe) in a given normal mode along the incident beam. As a stepping stone toward interpretation of the NRVS spectra for ferredoxins, N_2ase, and H_2ase, we have examined NRVS spectra for simple mononuclear and binuclear Fe complexes.

In this paper, we report ^{57}Fe NRVS data for the $FeCl_4^-$ ion in the solid state with NEt_4^+ or $P(C_6H_5)_4^+$ counterions, and for the $[Fe_2S_2Cl_4]^{2-}$ cluster with NEt_4^+ counterions (Chart 1). Raman and far-IR spectra for these materials are also presented. Normal-mode calculations are used to reproduce and interpret the experimental NRVS spectra. As both the frequency and the intensity of the NRVS bands can readily be calculated, there are sufficient constraints for a proper nonlinear least-squares optimization of Urey−Bradley force constants. Inclusion of the counterions was essential for interpretation of the complete spectra. The results are compared with previous models for these and related complexes.

The theory behind NRVS has been reviewed elsewhere;[14,15] here, we present the important results that relate this measurement to more familiar vibrational spectroscopies. A key quantity for the interpretation of NRVS spectra is $\vec{e}_{j\alpha}^{\,2}$, the "mode composition factor" for atom j in mode α.[16] The quantity $\vec{e}_{j\alpha}$ is used to create linear combinations of mass-weighted Cartesian displacements $\vec{r}_j$ of the jth atoms with masses m_j that correspond to the normal-mode displacements Q_α

$$Q_\alpha = \sum_j \vec{e}_{j\alpha} \cdot \vec{r}_j \sqrt{m_j} \tag{1}$$

If one begins with the normal modes, the mode composition factors can be extracted from the atomic displacements via[15]

$$\vec{e}_{j\alpha}^{\,2} = \frac{m_j r_j^{\,2}}{\sum_j m_j r_j^{\,2}} \tag{2}$$

In an NRVS experiment, for a particular eigenvector Q_α, the fraction of the integrated cross section is given by[17]

$$\phi(\omega) = \langle (\vec{e}_{\mathrm{Fe},\alpha} \cdot \hat{k})^2 \rangle \frac{E_\mathrm{R}}{\hbar\omega} (\bar{n}_\alpha + 1) f \tag{3}$$

In this expression, $\hat{k}$ is a unit vector along the direction of photon propagation; $\bar{n}_\alpha = [\exp(hc\bar{\nu}_\alpha/k_\mathrm{B}T) - 1]^{-1}$ is the thermal occupation factor for a mode of frequency $\bar{\nu}_\alpha$ at temperature T;[15] the recoil energy is $E_\mathrm{R} = \hbar^2k^2/2m_\mathrm{Fe}$ or $\sim$1.96 meV; and the recoilless fraction f depends on $\langle x_\mathrm{Fe}^2 \rangle$, the mean square fluctuation of the Fe nucleus along the beam direction, via $f = \exp(-k^2\langle x_\mathrm{Fe}^2 \rangle)$. For cases where it is difficult to observe discrete NRVS transitions, it is useful to define an Fe partial vibrational density of states (PVDOS), $D_\mathrm{Fe}(\bar{\nu})$, using a line shape function $\mathrm{L}(\bar{\nu} - \bar{\nu}_\alpha)$[16]

$$D_\mathrm{Fe}(\bar{\nu}) = \sum_\alpha (\vec{e}_{\mathrm{Fe},\alpha} \cdot \vec{k})^2 \mathrm{L}(\bar{\nu} - \bar{\nu}_\alpha) \tag{4}$$

The one-phonon NRVS excitation probability $S_1(\bar{\nu})$ is then proportional to $D(\bar{\nu})$ via

$$S_1(\bar{\nu}) = [\bar{n}(\bar{\nu}) + 1] \frac{\bar{\nu}_\mathrm{R}}{\bar{\nu}} D_\mathrm{Fe}(\bar{\nu}) \tag{5}$$

where $\bar{\nu}_\mathrm{R}$ is the recoil energy.

As described by Chumakov and co-workers,[18] if one assumes total decoupling of inter- and intramolecular vibrations, then in the acoustic modes, the mean square displacements of all the atoms are the same, and (assuming Fe is the resonant nucleus) the mode composition factor for each acoustic mode is given by

(13) Alp, E.; Sturhahn, W.; Toellner, T. S.; Zhao, J.; Hu, M.; Brown, D. E. *Hyperfine Interact.* **2002**, *144/145*, 3−20.
(14) Sturhahn, W. *J. Phys.: Condens. Matter* **2004**, *16*, S497−S530.
(15) Leu, B. M.; Zgierski, M. Z.; Wyllie, G. R. A.; Scheidt, W. R.; Sturhahn, W.; Alp, E. E.; Durbin, S. M.; Sage, J. T. *J. Am. Chem. Soc.* **2004**, *126*, 4211−4227.
(16) Sage, J. T.; Paxson, C.; Wyllie, G. R. A.; Sturhahn, W.; Durbin, S. M.; Champion, P. M.; Alp, E. E.; Scheidt, W. R. *J. Phys.: Condens. Matter* **2001**, *13*, 7707−7722.
(17) Sage, J. T.; Durbin, S. M.; Sturhahn, W.; Wharton, D. C.; Champion, P. M.; Hession, P.; Sutter, J.; Alp, E. E. *Phys. Rev. Lett.* **2001**, *86*, 4966−4969.
(18) Chumakov, A. I.; Rüffer, R.; Leupold, O.; Sergueev, I. *Struct. Chem.* **2003**, *14*, 109−119.

$$\vec{e}^{\,2}_{\text{acoustic}} = \frac{m_{\text{Fe}}}{\sum_j m_j} \tag{6}$$

Another useful formula supposes that the structure can be described in terms of two rigid molecular fragments, with the ^{57}Fe in a fragment with mass M_1, in which case the stretching mode composition factor is[18]

$$\vec{e}^{\,2}_{\text{stretch}} = \frac{m_{\text{Fe}}(\sum_j m_j - M_1)}{M_1 \sum_j m_j} \tag{7}$$

NRVS has already been used to study the dynamics of hemes in proteins[17] or as isolated porphyrin complexes,[15,16,19−21] the properties of Fe under extreme pressure,[22] thin films,[23] and Fe spin-state transitions.[24] Preliminary results on Fe−S complexes in rubredoxin[25] and Fe_4S_4 clusters[26] have also been reported. Because it has the resolution and information content of a vibrational spectroscopy, NRVS has the potential for characterization of catalytic intermediates in Fe-containing metalloenzymes such as nitrogenase,[27] hydrogenase,[28,29] cytochrome P-450,[30] and methane monooxygenase.[31]

Experimental Section

Sample Preparation. (i) $^{57}FeCl_3$. ^{57}Fe (55.8 mg, 1.00 mmol) was loaded in a three-neck round-bottom flask, and 150 mL of concentrated HCl(aq) was then added. The solution turned from a creamy color to a pale yellow. The mixture was set to reflux at 120 °C for 36 h. The yellow solution was then concentrated under reduced pressure until near dryness to give a slurry of brown-yellow $^{57}FeCl_3$.

(ii) [NEt$_4$][^{57}FeCl$_4$]. To the brown-yellow $^{57}FeCl_3$ prepared in the previous step was added 100 mL of ethanol, and the suspension was stirred for 1 h before it was filtered. The resulting yellow filtrate was reduced to 10 mL under reduced pressure. [NEt$_4$]C (165.71 mg, 1 mmol) was then added to the solution, and the reaction mixture was stirred for 1 h. Then, 0.2 g of [NEt$_4$][^{57}FeCl$_4$] (64% overall yield, based on ^{57}Fe) was isolated after filtration as a yellow powder.

(iii) [P(C$_6$H$_{54}$][^{57}FeCl$_4$]. [P(C$_6$H$_5$)$_4$][^{57}FeCl$_4$] was synthesized by the same procedure as used for [NEt$_4$][^{57}FeCl$_4$], except that 1 equiv of [P(C$_6$H$_5$)$_4$]Cl was used instead of 1 equiv of [NEt$_4$]Cl.

(iv) [NEt$_4$]$_2$[^{57}Fe$_2$S$_2$Cl$_4$]. [NEt$_4$]$_2$[^{57}Fe$_2$S$_2$Cl$_4$] was synthesized from [NEt$_4$][^{57}FeCl$_4$] and (Me$_3$Si)$_2$S according to published methods[32,33] after slight modifications. The samples were loaded into $3 \times 7 \times 1$ mm^3 (interior dimensions) Lucite cuvettes while in an anaerobic N_2-containing glovebox with an O_2 concentration of <0.1 ppm.

NRVS Measurements. ^{57}Fe NRVS spectra were recorded using standard procedures[14] on multiple occasions at beamline 3-ID at the Advanced Photon Source.[34] The monochromated photon flux was $\sim 2.5 \times 10^9$ photons/s in a 1.0 meV bandwidth at 14.4 keV in a 1 mm × 3 mm spot. The 3-ID monochromator consists of a water-cooled diamond (111) double-crystal monochromator with 1.1 eV band-pass, followed by two Si channel-cut crystals, mounted on high-precision rotation stages (Kohzu KTG-15AP) in a symmetric geometry. The first two crystals use Si(4,0,0) reflections; the latter two use the highest-order reflection possible (10,6,4) at 14.4125 keV.[35] During all NRVS measurements, the samples were maintained at cryogenic temperatures using a liquid He cryostat. Because the cryostat temperature sensors were not directly in contact with the samples, relevant temperatures for individual spectra were calculated from the ratio of anti-Stokes to Stokes intensities.[14] NRVS data were generally recorded between −20 and 75 meV in ∼45-min scans (4−20 scans per sample). Delayed nuclear fluorescence and Fe K fluorescence were recorded with an APD detector.[14,36] For [NEt$_4$][FeCl$_4$], the typical ^{57}Fe elastic signal count rate was ∼2000 cps.

Resonance Raman Spectroscopy. Raman samples were prepared as KBr pellets in an anaerobic glovebox. Spectra were recorded in backscattering geometry with a SPEX 1877 triple spectrometer, using ∼25 mW excitation at 488 nm by a Coherent Innova 70−2 Ar^+/Kr^+ laser and a cooled Spectrum One 594 CCD detector. During measurements, the samples were maintained at 77 K by immersion in liquid N_2 inside a quartz dewar. Spectra were calibrated by reference to a liquid CCl_4 spectrum using the bands at 218 and 314 cm^{-1}; slits were set for 3 cm^{-1} resolution.

FT-IR Spectroscopy. FT-IR samples were prepared as Nujol mulls in an anaerobic glovebox. Far-infrared absorption spectra were recorded at room temperature using a Brücker IFS 66 v/S FT-IR spectrometer with a Mylar beam splitter and a liquid He cooled Si bolometer. The sample chamber was evacuated to 1 mTorr to minimize the absorption by water vapor, and the energy resolution was 4 cm^{-1}.

NRVS Data Analysis and Normal-Mode Calculations. The ^{57}Fe partial vibrational densities of states were extracted from the

(19) Rai, B. K.; Durbin, S. M.; Prohofsky, E. W.; Sage, J. T.; Wyllie, G. R. A.; Scheidt, W. R.; Sturhahn, W.; Alp, E. E. *Biophys. J.* **2002**, *82*, 2951−2963.
(20) Rai, B. K.; Durbin, S. M.; Prohofsky, E. W.; Sage, J. T.; Wyllie, G. R. A.; Scheidt, W. R.; Sturhahn, W.; Alp, E. E. *J. Am. Chem. Soc.* **2003**, *125*, 6927−6936.
(21) Budarz, T. E.; Prohofsky, E. W.; Durbin, S. M.; Sjodin, T.; Sage, J. T.; Sturhahn, W.; Alp, E. E. *J. Phys. Chem. B* **2003**, *107*, 11170−11177.
(22) Mao, H. K.; Xu, J.; Struzhkin, V. V.; Shu, J.; Hemley, R. J.; Sturhahn, W.; Hu, M. Y.; Alp, E. E.; Vocadlo, L.; Alfè, D.; Price, G. D.; Gillan, M. J.; Schwoerer-Böhning, M.; D. Häusermann; Eng, P.; Shen, G.; Giefers, H.; Lübbers, R.; Wortmann, G. *Science* **2001**, *292*, 914−916.
(23) Keune, W.; Ruckert, T.; Sahoo, B.; Sturhahn, W.; Toellner, T. S.; Alp, E. E.; Röhlsberger, R. *J. Phys.: Condens. Matter* **2004**, *16*, S379−S393.
(24) Paulsen, H.; Benda, R.; Herta, C.; Schünemann, V.; Chumakov, A. I.; Duelund, L.; Winkler, H.; Toftlund, H.; Trautwein, A. X. *Phys. Rev. Lett.* **2001**, *86*, 1351−1354.
(25) Bergmann, U.; Sturhahn, W.; Linn, D. E.; Jenney, F. E., Jr.; Adams, M. W. W.; Rupnik, K.; Hales, B. J.; Alp, E. E.; Mayse, A.; Cramer, S. P. *J. Am. Chem. Soc.* **2003**, *125*, 4016−4017.
(26) Oganesyan, V. S.; Barclay, J. E.; Hardy, S. M.; Evans, D. J.; Pickett, C. J.; Jayasooriya, U. A. *Chem. Commun.* **2004**, 214−215.
(27) Christiansen, J.; Dean, D. R.; Seefeldt, L. C. *Annu. Rev. Plant Phys. Plant Mol. Biol.* **2001**, *52*, 273−295.
(28) Nicolet, Y.; Cavazza, C.; Fontecilla-Camps, J. C. *J. Inorg. Biochem.* **2002**, *91*, 1−8.
(29) Evans, D. J.; Pickett, C. J. *Chem. Soc. Rev.* **2003**, *32*, 268−275.
(30) *Cytochrome P-450: Structure, Mechanism, and Biochemistry*; Ortiz de Montellano, P. R., Ed.; Plenum Press: New York, 1995.
(31) Kopp, D. A.; Lippard, S. J. *Curr. Opin. Chem. Biol.* **2002**, *6*, 568−576.
(32) Wong, G. B.; Bobrik, M. A.; Holm, R. H. *Inorg. Chem.* **1978**, *17*, 578−584.
(33) Do, Y.; Simhon, E. D.; Holm, R. H. *Inorg. Chem.* **1983**, *22*, 3809−3812.
(34) Toellner, T. *Hyperfine Interact.* **2000**, *125*, 3−28.
(35) Toellner, T. S.; Hu, M. Y.; Sturhahn, W.; Quast, K.; Alp, E. E. *Appl. Phys. Lett.* **1997**, *71*, 2112−2114.
(36) Baron, A. Q. R. *Hyperfine interact.* **2000**, *125*, 29−42.

raw averaged spectra using the PHOENIX software package,[37] applying the recorded monochromator line shape function from the APS. No smoothing was used for any of the spectra. Normal-mode calculations were done using a modification of the program Vibratz[38] and a Urey−Bradley force field.[39] The parameters for this force field determine the potential energy V according to[40]

$$V = \sum_i \left[\frac{1}{2}K_i(\Delta r_i)^2 + K_i'(\Delta r_i)\right] + \sum_i \left[\frac{1}{2}H_i r_{i\alpha}{}^2(\Delta\alpha_i)^2 + H_i' r_{i\alpha}(\Delta\alpha_i)\right] + \sum_i \left[\frac{1}{2}F_i(\Delta q_i)^2 + F_i' q_i(\Delta q_i)\right]$$

In the above equation, Δr_i, $\Delta\alpha_i$, and Δq_i are changes in bond lengths, bond angles, and distances between nonbonded atoms, respectively. As detailed elsewhere,[40] the Urey−Bradley potential can be reduced to dependence on three essential types of parameters (K, F, and H) by a change of variables and the assumption that $F' = -F/10$.

In the Vibratz program, the Urey−Bradley potential is converted to an equivalent quadratic force field, and the normal modes for the molecular or crystal structure are subsequently derived by solution of the secular equation $|\mathbf{FG} - \lambda\mathbf{E}| = 0$, where **F** is the force constant matrix, **G** contains reduced masses, **E** is the identity matrix, and λ represents eigenvalues that lead to the vibrational frequencies.[40,41] For our application, the mean square Fe motion in a given normal mode was calculated from the normal-mode eigenvectors. The calculations for $[NEt_4][^{57}FeCl_4]$ and $[P(C_6H_5)_4][^{57}FeCl_4]$ began with the Urey−Bradley parameters described by Avery and co-workers,[42] who, in turn, used matrix elements derived by Simanouti.[39] The normal-mode calculations for $[NEt_4]_2[^{57}Fe_2S_2Cl_4]$ also began with Fe−S parameters described by Yachandra and co-workers.[43]

Optimization of Urey−Bradley Parameters. One advantage of NRVS for normal-mode analysis is that the intensities can be directly related to the mean square Fe motion in a particular normal mode.[14] Thus, a complete normal-mode analysis needs to account for both NRVS frequencies and amplitudes. In contrast, the resonance Raman intensity depends in a complex manner on the absorption spectrum and the geometry of the excited state, and calculation of IR amplitudes requires assumptions about the true charges on the atoms in a complex.[40]

We chose to use as a goodness-of-fit measure the sum of the squares of the differences between the observed and calculated NRVS partial vibrational density of states spectrum. To simulate the ^{57}Fe PVDOS, Gaussian and Lorentzian components were generated at the calculated frequencies, with an amplitude determined by the Fe mode composition factor for a particular normal mode[17] and a FWHM determined by the particular beamline employed. We note that there are no adjustable scale factors in these simulations.

(37) Sturhahn, W. *Hyperfine Interact.* **2000**, *125*, 149−172.
(38) Dowty, E. *Phys. Chem. Mater.* **1987**, *14*, 67−138.
(39) Simanouti, T. *J. Chem. Phys.* **1949**, *17*, 245−248.
(40) Nakamoto, K. *Infrared and Raman Spectra of Inorganic and Coordination Compounds*, 5th ed.; John Wiley and Sons: New York, 1997.
(41) Cotton, F. A. *Chemical Applications of Group Theory*, 3rd ed.; Wiley-Interscience: New York, 1990.
(42) Avery, J. S.; Burbridge, C. D.; Goodgame, D. M. L. *Spectrochem. Acta* **1968**, *24A*, 1721−1726.
(43) Yachandra, V. K.; Hare, J.; Gewirth, A.; Czernuszewicz, R. S.; Kimura, T.; Holm, R. H.; Spiro, T. G. *J. Am. Chem. Soc.* **1983**, *105*, 6462−6468.

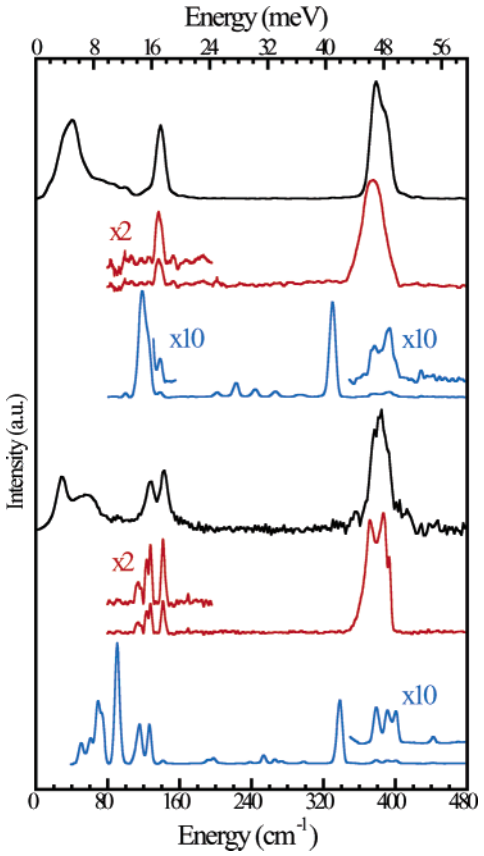

Figure 1. Upper group, top to bottom: ^{57}Fe PVDOS (black), FT-IR (red), and Raman (blue) spectra for $[NEt_4][^{57}FeCl_4]$. Lower group, top to bottom: ^{57}Fe PVDOS (black), FT-IR (red), and Raman (blue) spectra for $[P(C_6H_5)_4][^{57}FeCl_4]$.

Results and Discussion

The tetrahedral $FeCl_4^-$ ion presents about as simple a vibrational spectrum as possible for a transition metal complex. The IR and Raman spectra have been known for decades for the ion in ethereal solution,[44] as well as for the PCl_4^+ [45] and tetra-alkylammonium salts.[46] The normal modes have been simulated using modified Urey−Bradley force fields.[42] Quantitatively reproducing the NRVS of simple ions such as $FeCl_4^-$ seems advisable prior to modeling of the far more complex spectra of distorted tetrahedral Fe in rubredoxin or in biological Fe−S clusters.

$[NEt_4][^{57}FeCl_4]$. ^{57}Fe PVDOS spectra for $[NEt_4][^{57}FeCl_4]$ and $[P(C_6H_5)_4][^{57}FeCl_4]$ are presented in Figure 1 and Table 1, along with corresponding Raman and IR data. Three main peaks are observed in the $[NEt_4][^{57}FeCl_4]$ NRVS: clear intramolecular modes near 138 and 380 cm^{-1} and a possible lattice mode near 40 cm^{-1}. There is also residual NRVS intensity between 40 and 110 cm^{-1}. The highest-frequency modes have the greatest NRVS amplitude and hence the largest amount of Fe motion. In the T_d symmetry of an idealized isolated $^{57}FeCl_4^-$ anion, there is one A_1 totally symmetric stretching mode, along with one doubly degener-

(44) Woodward, L. A.; Singer, G. H. *J. Chem. Soc.* **1958**, 716−718.
(45) Kistenmacher, T. J.; Stucky, G. D. *Inorg. Chem.* **1968**, *7*, 2150−2155.
(46) Sabatini, A.; Sacconi, L. *J. Am. Chem. Soc.* **1964**, *86*, 17−20.

Table 1. Summary of NRVS, Raman, IR, and Calculations for $FeCl_4^-$ Salts

				Raman	FT-IR	^{57}Fe PVDOS		normal-mode calculation	
R	mode(s)	symmetry	type	ν (cm^{-1})	ν (cm^{-1})	ν (cm^{-1})	$\vec{e}_{Fe}^2$	ν (cm^{-1})	$\vec{e}_{Fe}^2$
NEt_4^+	ν_1	A_1	Fe−Cl stretch	330 330[a]	−	−	0	330[b]	0[b]
	ν_2	E	Fe−Cl bend	119 114[a]	−	−	0	118[b]	0[b]
	ν_3	T_2	Fe−Cl stretch	381[c] 372, 377, 394	∼376 ∼378[a]	∼380[c]	1.109	380[b]	1.354[b]
	ν_4	T_2	Fe−Cl bend lattice	139 138[a]	136 136[a]	∼138 40	0.463	133[b]	0.804[b]
$P\phi_4^+$	ν_1	A_1	Fe−Cl stretch	338	−	−	0	333	0
	ν_2	E	Fe−Cl bend	116	114	−	0	113	0
	ν_3	T_2	Fe−Cl stretch	390	381[c]	383	1.289	383	1.319
	ν_{3a}, ν_{3b}, ν_{3c}			378, 392, 401	372, 387, 392	376, 384, 391	1.289	371.5, 385.3, 386.6	1.319
	ν_4	T_2	Fe−Cl bend	127	131[c]	135	0.595	132[b]	0.892
	ν_{4a}, ν_{4b}, ν_{4c}				123, 128, 142	128, 142		128, 138, 142	0.892
			lattice	50, 60, 69		∼20−60		15.7−72.3	0.549

[a] Avery et al.[42] [b] Tetrahedral model. [c] Centroid.

ate E bend mode and two triply degenerate T_2 modes.[40] The NRVS features have to be assigned to T_2 modes, as Fe motion is excluded by symmetry for the A_1 and E modes.[40] By comparison with previous resonance Raman assignments,[42] we can say qualitatively that the ∼380 cm^{-1} band corresponds to a primarily Fe−Cl stretching motion and the ∼138 cm^{-1} band involves mostly Cl−Fe−Cl bending.

In T_d symmetry, only the T_2 modes are IR-active, and indeed, at moderate resolution, two T_2 bands are observed in the IR spectrum at 135 and ∼376 cm^{-1} (Figure 1). In principle, all of the modes could be Raman-active, but the strongest features are the E and A_1 modes seen at 120 and 330 cm^{-1}, respectively. At higher resolution, the former band reveals a shoulder at 129 cm^{-1}. With an expanded scale, both T_2 modes can be observed in the Raman spectrum (Figure 1), and the higher-frequency stretching band is observed to be split, with features at 372, 377, and 394 cm^{-1} in the natural-abundance spectrum. The NRVS peak in this region exhibits a high-energy shoulder at 392 cm^{-1} that presumably stems from the same splitting.

The effects of distortions from T_d symmetry have frequently been discussed in relation to the rubredoxin Fe site,[47] and this has been nicely illustrated by Vrajmasu and coworkers.[48] If the symmetry of the $FeCl_4^-$ anion were lowered to D_{2d}, the T_2 modes would split into E and B_2 modes, and the E modes descend to A_1 and B_1 representations.[40] Even lower symmetry is required to explain the splitting of the asymmetric stretch region into three components. However, the 40 cm^{-1} band cannot be explained simply in terms of distortion of the $FeCl_4^-$ ion; it is outside the range of any reasonable Cl−Fe−Cl bending mode. For example, a much more massive complex such as InI_4^- has an E mode at 42 cm^{-1}, but its T_2 mode is still at 58 cm^{-1}.[44] We therefore assign the intensity between 40 and 100 cm^{-1} to both acoustic and optical "lattice modes" involving motion of the entire $FeCl_4^-$ ion in or out of phase with the NEt_4^+ counterions.

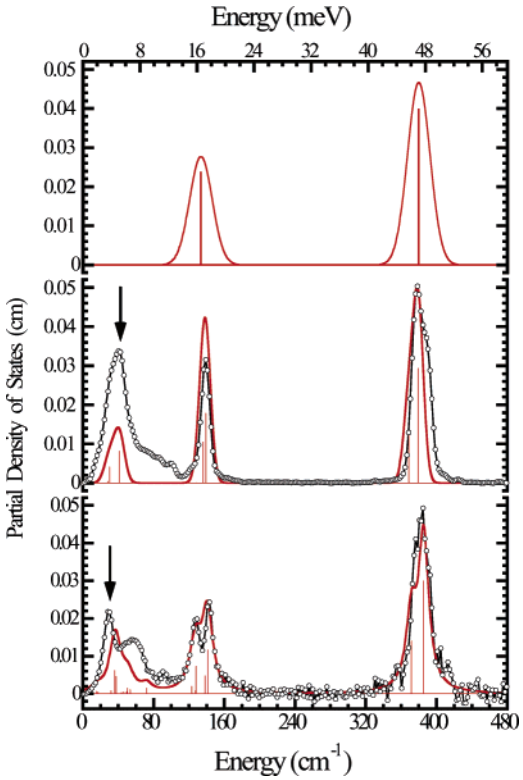

Figure 2. (Top) Simulation for isolated $FeCl_4^-$ anion assuming T_d symmetry (red). (Middle) APS ^{57}Fe PVDOS for $[NEt_4][FeCl_4]$ (points) and simulation based on crystal structure and point-mass cations (black). (Bottom) ^{57}Fe PVDOS for $[P(C_6H_5)_4][FeCl_4]$ (points) and simulation based on crystal structure (black). In all cases, sticks are proportional to mode composition factors of individual normal modes, and arrows correspond to the predicted upper limit of the acoustic modes.

(47) Yachandra, V. K.; Hare, J.; Moura, I.; Spiro, T. G. *J. Am. Chem. Soc.* **1983**, *105*, 6455−6461.
(48) Vrajmasu, V. V.; Bominaar, E. L.; Meyer, J.; Münck, E. *Inorg. Chem.* **2002**, *41*, 6358−6371.

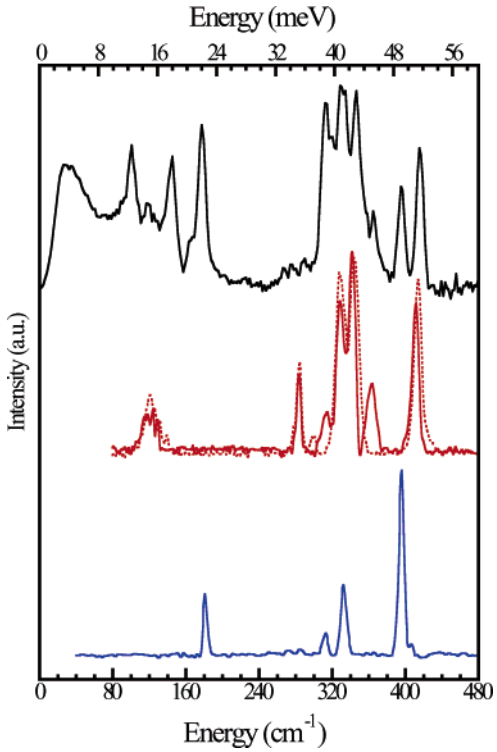

Figure 3. Spectra for $[NEt_4]_2[Fe_2S_2Cl_4]$. Top to bottom: $[NEt_4]_2[^{57}Fe_2S_2Cl_4]$ PVDOS (black), $[NEt_4]_2[^{57}Fe_2S_2Cl_4]$ FT-IR (red, solid) and natural-abundance $[NEt_4]_2[Fe_2S_2Cl_4]$ FT-IR (red, dotted), $[NEt_4]_2[^{57}Fe_2S_2Cl_4]$ Raman (blue).

We tested these assignments with normal-mode calculations using a Urey−Bradley force field.[40] First, we modeled the $FeCl_4^-$ ion in T_d symmetry and ignored the counterion. We optimized the force constants by minimizing the difference between calculated and observed Fe PVDOS. The resulting values, $K = 1.55$ mdyn/Å, $H = 0.030$ mdyn/Å, and $F = 0.17$ mdyn/Å, (F' fixed at $-F/10$), agreed well with previously reported values ($K = 1.51$ mdyn/Å, $H = 0.024$ mdyn/Å, $F = 0.19$ mdyn/Å, $F' = -0.008$ mdyn/Å). The predicted T_2 frequencies and intensities agree within ~4 cm^{-1} of the centroid values extracted from the NRVS spectrum (Table 1 and Figure 2). As summarized in Table 1, the frequencies of the NRVS-inactive A and E modes are also predicted within 2 cm^{-1}, even though they are not part of the NRVS analysis in T_d symmetry.

We then changed the model to include an entire $[NEt_4][^{57}FeCl_4]$ unit cell with the crystallographically disordered NEt_4^+ ions[49] modeled as point masses. With appropriate force constants, inclusion of a counterion introduces a cluster of low-frequency modes between 27 and 47 cm^{-1}. These $k = 0$ optical lattice modes account for about 25% of the low-frequency PVDOS, with $k \neq 0$ acoustic modes, which are not part of the normal-mode calculation, presumably making up the rest. Inclusion of the point counterion splits the intramolecular modes by up to 10 cm^{-1}.

The extent of the acoustic region of the spectrum can be estimated using procedures described by Chumakov and coworkers.[18] According to eq 6, the mode composition factor for the acoustic modes should be 17.3% of the total PVDOS. If the optical modes are first subtracted, then the integrated PVDOS reaches this value at 39.4 cm^{-1} in the recorded data as illustrated in Figure 2.

Chart 2. Symmetry Analysis of the 18 Normal Modes of a D_{2h} $X_2Y_2Z_4$ Molecule[40]

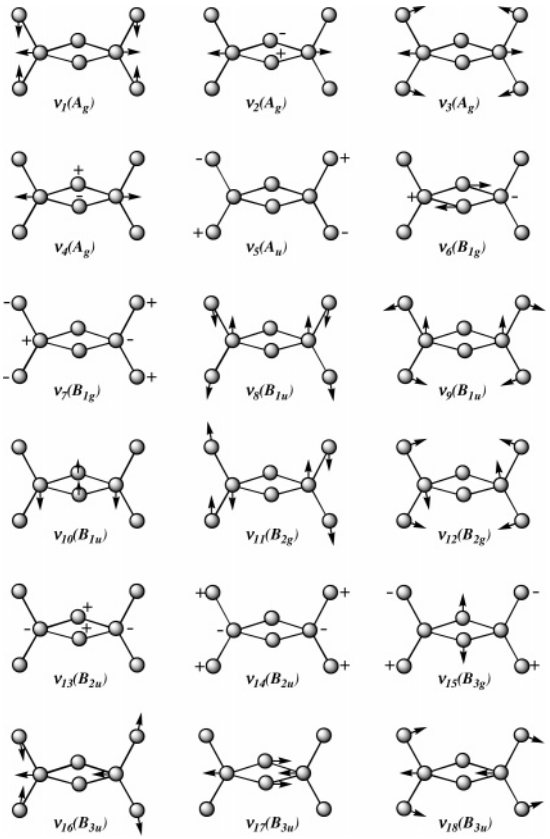

$[P(C_6H_5)_4][^{57}FeCl_4]$. To confirm this interpretation, we examined a salt with a more massive counterion, namely, $[P(C_6H_5)_4][^{57}FeCl_4]$ (Figure 1). A two-body point-mass model, that also assumes the same anion−cation force constants, predicts that the stretching frequency should be lower by the square root of the ratio of reduced masses, 0.6. In fact, the low-frequency maximum shifts from 40 to 24 cm^{-1}, exactly as predicted for the point-mass model. The observations are thus qualitatively in agreement with the assignment of the bands below 120 cm^{-1} as lattice modes.

However, the remainder of the $[P(C_6H_5)_4][^{57}FeCl_4]$ NRVS data exhibited some surprises, including a complex pattern in the stretching mode region around 380 cm^{-1} and splitting of the original T_2 bend mode region into two clear peaks near 128 and 142 cm^{-1} (Figure 1). The 142 cm^{-1} band is also seen in the far-infrared spectrum (Figure 1), and the lower 128 cm^{-1} band can be resolved into components at 123 and 128 cm^{-1}. In the low-frequency Raman spectrum, there are two distinct peaks at 115 and 127 cm^{-1}; the former mode might also be weakly seen in the NRVS and IR spectra. In the high-frequency Raman spectrum, the totally symmetric stretch has shifted to a slightly higher energy at 338 cm^{-1}, and the T_2 asymmetric Fe−Cl stretch splits into bands at 378, 392, and 401 cm^{-1}. At least five additional Raman bands are observed below 100 cm^{-1}; detailed interpretation is beyond the scope of this paper.

(49) Evans, D. J.; Hills, A.; Hughes, D. L.; Leigh, G. J. *Acta Crystallogr. C: Cryst. Struct. Commun.* **1990**, *46*, 1818−1821.

Table 2. Raman, FT-IR, NRVS, and D_{2h} Normal-Mode Analysis for $[NEt_4]_2[Fe_2S_2Cl_4]$

			Raman	FT-IR	NRVS		normal-mode analysis	
mode	symmetry	type	ν (cm^{-1})	ν (cm^{-1})	ν (cm^{-1})	$\vec{e}_{Fe}^2$	ν (cm^{-1})	$\vec{e}_{Fe}^2$
ν_1	A_g	Fe−S stretch	396 401[a]		396	0.21	395.4	0.18
ν_2	A_g	Fe−Cl stretch	313 318[a]		313	0.37	312.8	0.45
ν_3	A_g	Fe_2S_2 bend	180		177	0.38	176.6	0.34
ν_4	A_g	Fe−S ring bend	−		101	0.28	100.5	0.39
ν_5	A_u	Fe−Cl_2 twist	−	−	−	0	−	−
ν_6	B_{1g}	Fe−S stretch	−	−	337	0.29	343.4	0.46
ν_7	B_{1g}	Fe−Cl_2 wag	−	−	145	0.43	149.3	0.38
ν_8	B_{1u}	Fe−Cl stretch	−	328 334[a]	329	0.60	330.1	0.46
ν_9	B_{1u}	ring puckering and $FeCl_2$ rock	−	−	163	0.10	162.9	0.15
ν_{10}	B_{1u}	ring puckering	−	−	15−30	−	19.7	0.23
ν_{11}	B_{2g}	Fe−Cl stretch	332 331[a]	−	332	0.30	328.3	0.45
ν_{12}	B_{2g}	Fe−Cl_2 rock	−	−	96	0.37	102.4	0.024
ν_{13}	B_{2u}	Fe−S stretch	−	412 415[a]	415	0.30	408.3	0.38
ν_{14}	B_{2u}	Fe−Cl_2 wag	−	115	118	0.20	107.3	0.24
ν_{15}	B_{3g}	cluster twist	−	−	−	0	−	−
ν_{16}	B_{3u}	Fe−Cl stretch	−	342 345[a]	346	0.55	345.0	0.34
ν_{17}	B_{3u}	Fe−S stretch	−	284 287[a]	289	0.06	288.1	0.16
ν_{18}	B_{3u}	Cl−Fe−Cl bend	−	123	123	0.12	120.2	0.12

[a] Spiro et al.[43]

For a more quantitative analysis, we again conducted normal-mode calculations for an entire unit cell, this time with $P(C_6H_5)_4^+$ counterions. As illustrated in Table 1 and Figure 2, inclusion of counterion interactions results in a splitting of the T_2 bend mode region by up to 20 cm^{-1}. This simulation also captures the low-energy peak in the NRVS spectra with two peaks at 29 and 55 cm^{-1} and leaves little doubt as to the assignment of the lattice modes. As with the $[NEt_4][^{57}FeCl_4]$ spectrum, there are also "acoustic" modes with finite momentum that need to be considered. According to eq 6, the mode composition factor for the acoustic modes should be 10.6% of the PVDOS. If the optical modes are first subtracted, then the integrated PVDOS reaches this value at 36.1 cm^{-1}.

$[NEt_4]_2[Fe_2S_2Cl_4]$. The $[Fe_2S_2Cl_4]^{2-}$ anion is a binuclear metal cluster with approximate centrosymmetry in the NEt_4^+ salt,[50] whose Raman and IR modes have previously been studied in relation to 2Fe−2S ferredoxins.[43] Analysis of this complex is thus a reasonable stepping stone to more complex Fe−S clusters. The NRVS, Raman, and IR spectra for the $[NEt_4]_2[Fe_2S_2Cl_4]$ salt are presented in Figure 3. In D_{2h} symmetry, the 18 intramolecular vibrations divide into $4A_g$, $1A_u$, $2B_{1g}$, $3B_{1u}$, $2B_{2g}$, $2B_{2u}$, $1B_{3g}$, and $3B_{3u}$ normal modes,[40] as summarized in Chart 2. Of course, the true normal coordinates are linear combinations (within a symmetry class) of the pure terminal and bridging stretches and bends depicted in this chart.

Because of the inversion center, the "even" Raman-active modes are mutually exclusive with the "odd" IR-active modes; this is the general pattern seen in Figure 3. These conventional spectra are in accord with published results;[43] small (<5 cm^{-1}) differences are observed because of the use of ^{57}Fe instead of natural-abundance Fe. In addition, we were able to observe features below 250 cm^{-1} that were outside the range of prior work on $Fe_2S_2Cl_4^{2-}$.[43] For example, we attribute a strong Raman band at 180 cm^{-1} to a totally symmetric cluster bend mode. Similar modes were seen near 200 cm^{-1} in thiolate-ligated Fe_2S_2 clusters by Han et al.,[51] who assigned them as totally symmetric bends as well. The IR features around 120 cm^{-1} have also not been reported previously. Overall, the ^{57}Fe PVDOS spectrum for $[NEt_4]_2[Fe_2S_2Cl_4]$ (Figure 3) corresponds well with the Raman and IR data, including the newly observed low-frequency modes.

Initial normal-mode assignments were based on the previous study by Yachandra and co-workers.[43] However, we used the more conventional symmetry assignments for D_{2h} $X_2Y_2Z_4$ molecules,[40] with the *x* axis defined by the Fe−Fe vector, the *y* axis defined by the S−S vector, and the *z* axis perpendicular to the Fe_2S_2 plane.[40] The observed frequencies and amplitudes are summarized in Table 2, along with the normal-mode assignments. In contrast to the eight or nine modes allowed for IR or Raman, respectively, 16 modes are predicted to involve Fe motion and hence exhibit ^{57}Fe NRVS intensity (Chart 2). (The B_{3g} mode is NRVS-inactive, and the A_u mode is invisible to all three techniques.)

To simulate the ^{57}Fe PVDOS, we began with published Fe−S force constants,[43] as well as values for Fe−Cl interactions derived earlier. Because our data extend to lower frequencies, we were able to add a force constant for Fe−S−Fe−Cl torsion (Table 3). After refining these parameters

(50) Bobrik, M. A.; Hodgson, K. O.; Holm, R. H. *Inorg. Chem.* **1977**, *16*, 1851−1858.

(51) Han, S.; Czernuszewicz, R. S.; Spiro, T. G. *J. Am. Chem. Soc.* **1989**, *111*, 3496−3504.

Table 3. Summary of Urey−Bradley Force Constants for $FeCl_4^-$ and $Fe_2S_2Cl_4^{2-}$ [a]

sample	K (mdyn/Å)		H (mdyn/Å)		F (mdyn/Å)	
$[NEt_4][FeCl_4]$	Fe−Cl	1.51[b]	Cl−Fe−Cl	0.024[b]	Cl···Cl	0.19[b]
		1.55		0.03		0.168
$[P(C_6H_5)_4][FeCl_4]$	Fe−Cl	1.55	Cl−Fe−Cl	0.12	Cl···Cl	0.168
$[NEt_4]_2[Fe_2S_2Cl_4]$	Fe−S	1.44[c]	S−Fe−S	0.25[c]	S···S	0.05[c]
		1.45		0.19		0.08
	Fe−Cl	1.16	S−Fe−Cl	0.21	S···Cl	0.08
	Fe−Fe	0.40	Cl−Fe−Cl	0.23	Cl···Cl	0.08
			Fe−S−Fe	0.27[c]		
				0.35		
			Fe−S−Fe−Cl torsion	0.015		

[a] Values without superscripts are from this work. [b] Avery et al.[42] [c] Yachandra et al.[43]

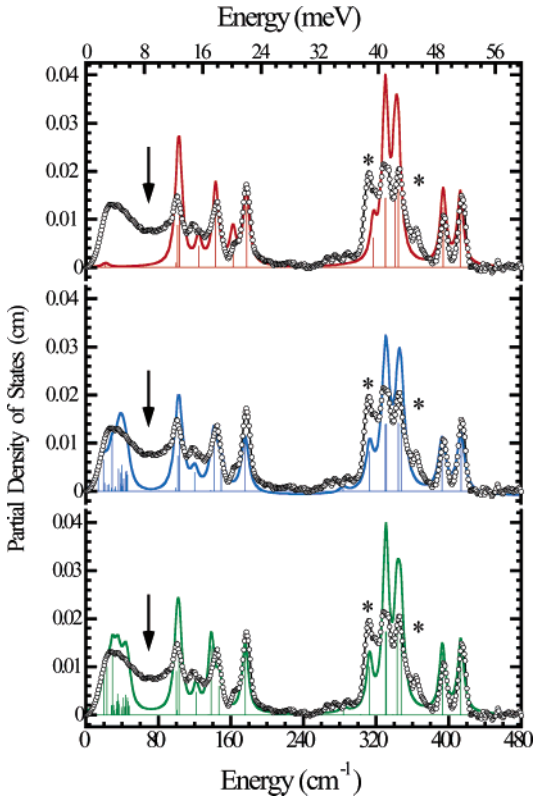

Figure 4. (Top) PVDOS (points) and simulation (black) for isolated $[^{57}Fe_2S_2Cl_4]^{2-}$ anion assuming D_{2h} symmetry. Sticks are proportional to mode composition factors of normal modes. (Middle) ^{57}Fe PVDOS (points) and simulation (black) for $[NEt_4]_2[^{57}Fe_2S_2Cl_4]$ based on crystal structure and using point masses for cations. (Bottom) PVDOS (points) and simulation (black) for $[NEt_4]_2[^{57}Fe_2S_2Cl_4]$ using complete cation structures. The peaks marked by asterisks (*) are presumed to derive mostly from impurities. In all cases, sticks are proportional to mode composition factors of individual normal modes, and arrows correspond to the predicted upper limit of the acoustic modes.

to best reproduce the ^{57}Fe PVDOS, the D_{2h} simulation captures nearly all of the intramolecular features above 100 cm^{-1} (Figure 4).

Among the well-resolved bands that are accurately reproduced in both frequency and amplitude, we point to the asymmetric (B_{2u}) and symmetric (A_g) Fe−S stretches at 415 and 396 cm^{-1}, respectively; the A_g mode at 177 cm^{-1}; and a B_{3u} mode at ∼286 cm^{-1} that is more clearly seen in the IR data (Figure 3). The atomic motions involved in these modes are illustrated in Figure 5. At the lower-frequency

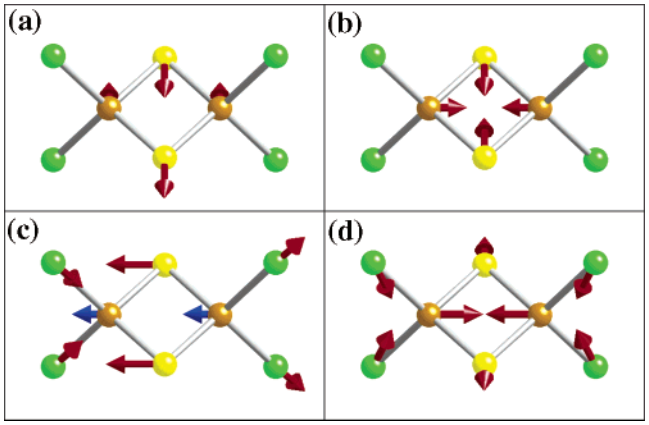

Figure 5. Illustration of relative atomic motions in normal modes deduced from simulations: (a) asymmetric (B_{2u}) Fe−S stretch at 415 cm^{-1} (b) symmetric (A_g) Fe−S stretch at 396 cm^{-1}, (c) B_{3u} mode at ∼288 cm^{-1}, (d) symmetric A_g ring bend mode at 177 cm^{-1}. Red arrows are at ×2 and blue arrows are at ×10 magnification of relative atomic displacements.

limit, the calculations predict a B_{1u} mode at 19.7 cm^{-1}. Frey and co-workers observed a B_{1u} "$FeCl_2$ rock/ring puckering" mode at 24 cm^{-1} in the IR spectrum of Fe_2Cl_6 isolated in an Ar matrix.[52]

The observed intensity in the low-energy region is still greater than predicted for the isolated anion. It was shown earlier with the (R)$[FeCl_4]$ spectra that the region below 100 cm^{-1} includes lattice modes and inclusion of the counterion is required for a good simulation. As seen in Figure 4, by incorporating the NEt_4^+ cations as point masses in a simulation for $[NEt_4]_2[Fe_2S_2Cl_4]$, a large number of low-frequency modes are generated. However, even with inclusion of optical lattice modes, the simulations only account for roughly 35% of the NRVS intensity. As before, the remainder can be attributed to acoustic modes. Again, using eq 6, the mode composition factor for the acoustic modes should be 19.6% of the PVDOS, and the integrated PVDOS reaches this value at 43.6 cm^{-1}.

The greatest discrepancy between observed and calculated spectra occurs for the band at 365 cm^{-1}, which is not reproduced by the normal-mode calculations. There is also significantly more intensity in the experimental PVDOS around 310 cm^{-1} than is seen in the simulations. An explanation for this discrepancy can be derived from the IR spectra of two different samples, i.e., the ^{57}Fe-enriched $[NEt_4]_2[Fe_2S_2Cl_4]$ sample that was prepared on a small scale and a recrystallized unenriched $[NEt_4]_2[Fe_2S_2Cl_4]$ sample that was produced on a larger scale (Figure 3). The problematic IR bands at ∼310 and 365 cm^{-1} are not seen in the latter sample; they are presumed to derive from impurities in our ^{57}Fe-enriched sample.

Summary and Conclusions

The reported results show that the NRVS spectra for mononuclear and binuclear Fe complexes can be quantitatively reproduced by normal-mode calculations with a Urey−Bradley force field. Combined with the fact that the NRVS

(52) Frey, R. A.; Werder, R. D.; Günthard, H. H. *J. Mol. Spectrosc.* **1970**, *35*, 260−284.

amplitudes are also amenable to straightforward calculation, these spectra often provide more constraints than available from IR or Raman data alone. For the complexes used in this study, this meant that a nonlinear least-squares refinement was possible without the necessity of additional isotope substitution of the non-Fe atoms. In contrast, the generalized valence force field analysis of conventional vibrational spectra is often highly underdetermined with the available constraints.

The Urey−Bradley parameters could be converted into a generalized valence force field for a quantitative comparison with predictions from DFT calculations. Of course, all molecular force fields suffer from the limits of these inherently nonquantum mechanical models. Alternatively, the Fe PVDOS experimental data could itself be compared directly with results from quantum mechanical calculations. One question for further study of Fe−S clusters is: Can iteration between vibrational properties observed in the NRVS experiment and DFT calculations be used to predict or refine structures? In some cases, NRVS might be used to detect cluster properties that are difficult to discern in X-ray crystallographic analyses. For example, the low-frequency bend modes are quite sensitive to local symmetry: simply changing the counterion in $[NEt_4]FeCl_4$ to $[P(C_6H_5)_4]^+$ resulted in a significant splitting in the T_2 bending mode in a spectral region that is difficult to study in proteins. The bend/torsion region around 100 cm^{-1}, which is often ignored for Fe−S clusters, was also found to be extremely sensitive to the local environment of the Fe complex.

For the current study, we chose complexes that were also amenable to Raman and IR spectroscopies. One powerful application of the NRVS technique will be the study of Fe−S clusters at redox levels that have proven intractable for resonance Raman spectroscopy, such as reduced rubredoxins and all-ferrous Fe_4S_4 clusters. The technique will also permit observation of many modes that are outside the range of solution FT-IR measurements.

For elements with appropriate nuclear resonances, NRVS is gradually becoming appreciated as a powerful complement to IR, Raman, and inelastic neutron spectroscopies. It already has sufficient sensitivity to allow study of metalloproteins, and the main barrier to broader use is the relatively small number of beamlines available. As synchrotron radiation facilities expand and evolve, NRVS should make an important contribution to a wide range of chemical and biological problems.

Acknowledgment. We thank Dr. Thomas Toellner at the APS and Mr. Philip Titler for assistance with our experiments. This work was funded by NIH grants GM-65440 (S.P.C.), GM-44380/EB001962 (S.P.C.), and GM-33080 (D.C.) and the DOE Office of Biological and Environmental Research (S.P.C.). Use of the Advanced Photon Source is supported by the U.S. Department of Energy, Basic Energy Sciences; Office of Science, under Contract W-31-1-9-Eng-38.

IC0482584